

THREE-DIMENSIONAL MICROMECHANICS-BASED CONSTITUTIVE FRAMEWORK FOR ANALYSIS OF PULTRUDED COMPOSITE STRUCTURES

By Rami Haj-Ali,¹ Hakan Kilic,² and Abdul-Hamid Zureick³

ABSTRACT: A new 3D micromechanics-based framework is proposed for the nonlinear analysis of pultruded fiber-reinforced polymeric composites. The proposed 3D modeling framework is a nested multiscale approach that explicitly recognizes the response of the composite systems (layers) within the cross section of the pultruded member. These layers can have reinforcements in the form of roving, continuous filament mat (CFM), and/or woven fabrics. Different 3D micromechanical models for the layers can be used to recognize the basic response of the fiber and matrix materials. The framework is implemented with both shell and 3D finite elements. The 3D lamination theory is used to generate a homogenized nonlinear effective response for a through-thickness representative stacking sequence. The proposed modeling framework for pultruded composites is used to predict the stiffness and nonlinear stress-strain response of E-glass/vinylester pultruded materials reinforced with roving and CFM. The roving layer is idealized using a 3D nonlinear micromechanics model for a unidirectional fiber-reinforced material. A simple nonlinear micromechanics model for the CFM layer is also applied. The proposed model shows very good predictive capabilities of the overall effective properties and the nonlinear response of pultruded composites, based on the in situ material properties, and the volume fractions of the constituents. Experimental data from off-axis tests of pultruded plates under uniaxial compression are used to verify the proposed model. The proposed framework can be easily incorporated within displacement-based finite-element models of composite structures.

INTRODUCTION

Pultruded fiber-reinforced polymeric (FRP) structural members are currently used in a number of structural applications. These composite members are prismatic and can have a general cross-sectional shape. They are heterogeneous composites that combine different forms of reinforcement systems that are repeated through the thickness of the member. Pultruded composite plates or beams are relatively thick structural members with a small number of reinforcement layers. Different combinations of reinforcements, such as roving, CFM, woven fabrics, and braided preforms, can be used in the pultrusion process, with CFM and roving being the most commonly used. The CFM consists of relatively long and swirl fibers that are randomly oriented (in plane). CFM is usually used in pultruded members as a multidirectional secondary reinforcement system, and providing for material continuity in transition regions within the cross sections, e.g., near the web-flange junction in an I-shape pultruded member.

Many experimental studies have been carried out to characterize the material properties and the response of pultruded composites. Herakovich and Mirzadeh (1991) studied the fiber spacing and the resin-rich areas in a pultruded graphite/epoxy composite. They concluded that the nonuniform fiber spacing and fiber waviness in this material can lead to a reduction in stiffness and strength. Binshan et al. (1995) performed a series of tests on the determination of fiber volume fractions (FVF) in pultruded specimens cut from standard profiles, plates, gratings, and rebars. Void content is relatively high in pultruded materials compared to composites made in an autoclave from preimpregnated tape or using resin transfer molding techniques. Wang and Zureick (1994) conducted a study to char-

acterize the tensile behavior of coupon specimens cut from different locations of a pultruded I-shape beam. They showed that a significant number of voids existed in these coupons, and that the roving reinforcement was found unevenly distributed.

Mottram (1992) conducted an experimental study on the design of pultruded I-beams subject to lateral-torsional buckling. This study indicates the need to include shear deformation effects in the buckling analysis of pultruded FRP beams. Mottram (1993) investigated the buckling behavior of pultruded closed sections that are fabricated by adhesively bonding I- and channel sections. The stiffness of the assembly from three-point bending tests is found to be 7% lower than the predicted value calculated using elastic beam theory. Mottram attributed the difference to the variation of section properties and the effect of adhesive bonding. Turvey (1998) performed several tests to investigate the behavior of pultruded glass-reinforced plastic sheet under torsion. Coupons with various lengths are cut parallel and transverse to the pultrusion direction of the sheet, in order to obtain material properties for calculating torsional stiffness and strength. In the case of specimens with shorter span length, observed torsional stiffness for the transverse coupons is significantly lower than the longitudinal ones. On the other hand, there is no significant difference in stiffness in the case of long specimens. Moreover, the failure torque and twist values are higher in longitudinal coupons than the transverse ones.

Finite element (FE) structural models have been applied to pultruded composite structures. Most of these studies consider the material to be linear orthotropic and homogeneous. Bank and Yin (1999) investigated the postbuckling regime of pultruded I-beams, focusing on the web-flange junction failure. They performed a finite-element analysis using a node separation technique to simulate the local separation of the flange from the web following local buckling of the flange. Smith et al. (1998, 1999) performed a detailed shell FE analysis of a proposed connection design and proposed a condensation method for the effective moment-rotation response of the connection. Zureick et al. (1995) examined the experimental and analytical behavior of I-shape pultruded FRP deep beams subject to transverse loads in the plane of the web. Vakanier et al. (1991) performed linearized buckling analysis of an axially compressed pultruded stocky section using FE models to investigate local flange buckling.

¹Asst. Prof., School of Civ. and Envir. Engrg., Georgia Inst. of Technol., Atlanta, GA 30332-0355. E-mail: rami.haj-ali@ce.gatech.edu

²PhD Candidate, School of Civ. and Envir. Engrg., Georgia Inst. of Technol., Atlanta, GA 30332-0355. E-mail: hkilic@nora.ce.gatech.edu

³Prof., School of Civ. and Envir. Engrg., Georgia Inst. of Technol., Atlanta, GA 30332-0355. E-mail: azureick@ce.gatech.edu

Note. Associate Editor: George Voyiadjis. Discussion open until December 1, 2001. To extend the closing date one month, a written request must be filed with the ASCE Manager of Journals. The manuscript for this paper was submitted for review and possible publication on March 6, 2001; revised March 21, 2001. This paper is part of the *Journal of Engineering Mechanics*, Vol. 127, No. 7, July, 2001. ©ASCE, ISSN 0733-9399/01/0007-0653-0660/\$8.00 + \$.50 per page. Paper No. 22676.

A micromechanical modeling approach to generate the overall effective stiffness of pultruded composite material systems has been proposed (Barbero 1991; Sonti and Barbero 1996). The modeling approach employs the periodic microstructure formulas of Luciano and Barbero (1994), the classical lamination theory, and mechanics of laminated beams, respectively, to determine the overall effective stiffness of pultruded composite beams. The needed in-plane stiffness for the CFM layers is generated from approximate expressions proposed by Tsai and Pagano (1968). Their overall stiffness prediction compared well with their experimental results.

Pultruded structural members may exhibit a nonlinear structural response when subjected to external loading. This is primarily due to the soft response of the polymeric matrix and to the presence of voids and microcracks. Nonlinear effects may also occur at low load levels near geometric and material discontinuities. These localized nonlinear effects will influence the overall structural response as the load increases. The state of deformation at these critical locations can significantly influence the structural response and mode of failure. Thus, there exists a need for detailed 3D micromechanics-based nonlinear models capable of predicting the material response under a general multiaxial state of loading.

This study presents a new 3D micromechanics-based framework for nonlinear analysis of FRP pultruded composites. The proposed 3D modeling framework is a nested multiscale micromechanical approach that explicitly recognizes the responses of the different composite systems (layers). To this end, a sublaminar model is used to generate an equivalent continuum response for a material point within the cross section of the pultruded member. Different 3D micromechanical models can be used to represent the composite systems within the sublaminar; these layers include roving, CFM, and woven composites. The 3D micromodels for the different layers recognize the basic response of the fiber and matrix materials.

The first part of this paper describes the different elements in the proposed model. A formulation is then presented for the homogenization methods with the nonlinear 3D micromechanical models for the sublaminar, roving, and CFM material systems. A simple calibration procedure for the properties of the fiber and the matrix constituents (stiffness, FVF, and non-

linear uniaxial response of the matrix) is also presented. Finally, the model's ability to predict the elastic stiffness and nonlinear stress-strain response different glass-vinylester coupons with varying off-axis angles of the roving reinforcement is examined.

PULTRUDED COMPOSITE MATERIAL

The pultruded composite material modeled in this study consists of a resin system reinforced with unidirectional roving and continuous filament mats. Fig. 1 is a magnified view of the cross section of a 12.7 mm (1/2-in.) thick plate. The CFM system can be idealized as a layered medium, with relatively long and swirly fibers that are randomly oriented in the plane. However, the roving system is a collection of fiber bundles that are distributed in designated locations within the medium (idealized as a roving layer). The CFM and roving layers can have different thicknesses throughout the cross section. The pultruded material used in this study is made from E-glass fibers and a vinylester matrix. The material is idealized as a perfectly bonded layer system consisting of roving and CFM layers. In addition to these constituents, there is an appreciable number of voids spread inside the pultruded section as reported by Haj-Ali et al. (1998). These voids tend to concentrate at the center of the section. The FVFs of unidirectional roving and CFM are determined by a burnout test, and are 0.407 for the roving and 0.305 for the CFM. These are average FVF values of all the roving and CFM layers, respectively. The total average E-glass FVF in the material (from both the roving and CFM volumes) is 34%.

NESTED MICROMECHANICAL MODELING FRAMEWORK

The 3D micromechanical framework, integrated with FE models for pultruded composite structures, is schematically illustrated in Fig. 2. It describes a number of nested micromodels for each of the composite systems that exist within the material. This material modeling framework is general and can be integrated with a shell type or 3D continuum finite-element models for pultruded structures. The nonlinear response of the pultruded structures is sampled at material points (Gaussian

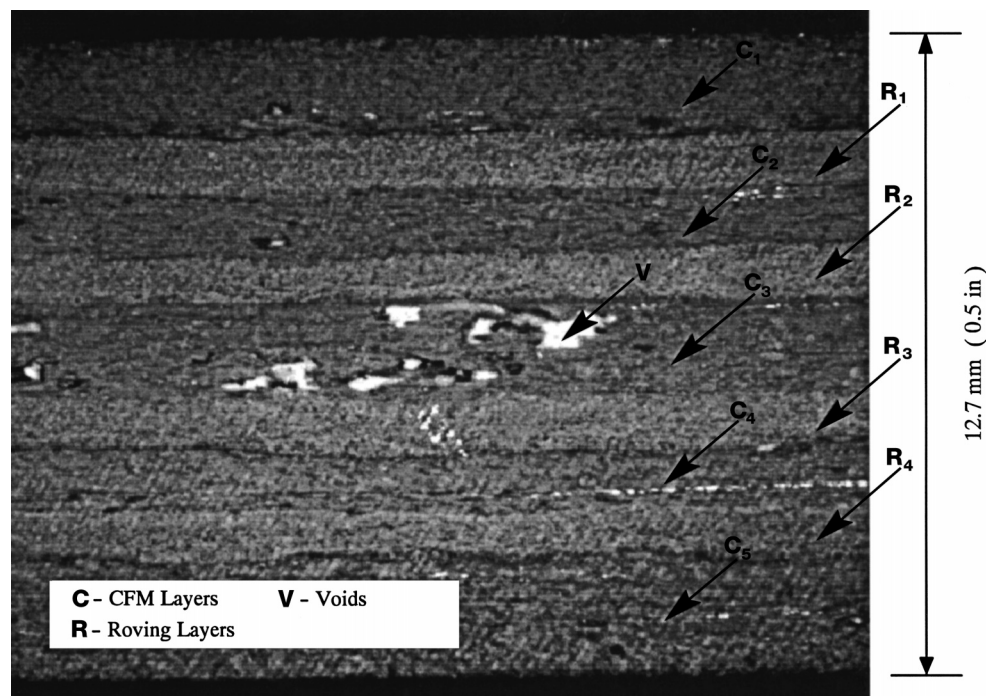


FIG. 1. Cross Section of Glass/Vinylester Pultruded Composite Plate

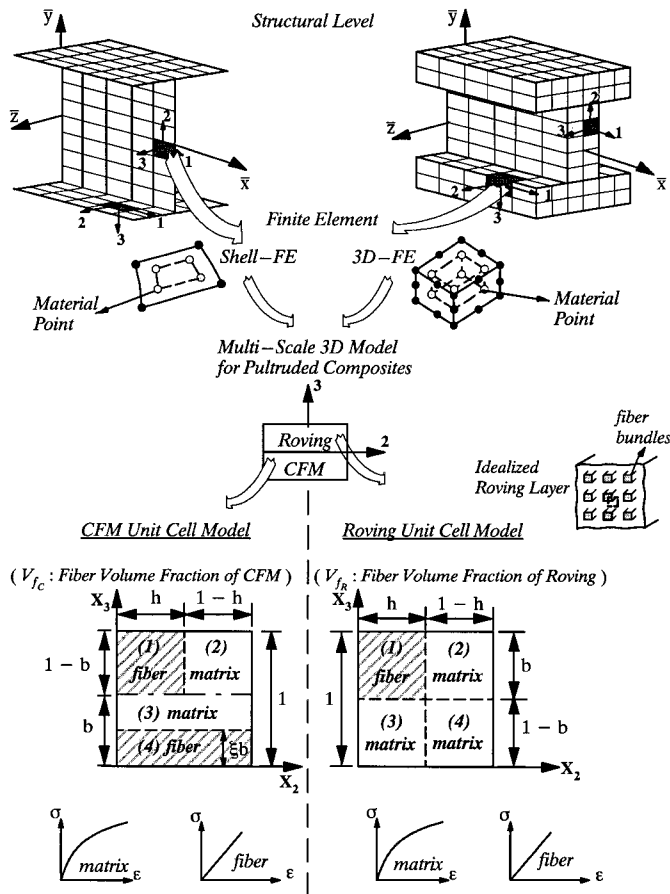


FIG. 2. Framework for 3D Nonlinear Analysis of Pultruded Composite Structures

integration points) within the elements in the FE model. The equivalent response, at a material point in 3D FE models, represents a homogenized equivalent continuum response for a repeated stacking sequence through the thickness of each element. This level of the model is referred to as the sublaminate model. It employs the 3D lamination theory to generate a nonlinear continuum response for the CFM and the roving layers, following the nonlinear general formulation of Haj-Ali and Pecknold (1996). The homogenization is performed at each material point in the thickness direction, the third axis in the local material orientation system attached with each finite element, as shown in Fig. 2. In the case where a shell-type FE model is used to model the pultruded structure, the micro-mechanical framework may not include the sublaminate model. Instead, the response of the cross section is generated by a through-thickness ply-by-ply integration of the response of each individual layer. A state of plane-stress condition is assumed to exist in each of the CFMs and roving layers that span the cross section. The 3D lamination theory, in this case, is reduced to the well-known classical lamination theory.

Two independent 3D micromechanical material models are used for the roving and CFM layers. The first is a unit-cell (UC) micromechanical model for the unidirectional roving layers. This model is derived in terms of average stresses and strains in the four subcells, similar to the method of cells micromodel proposed by Aboudi (1991). The second is a simple 3D micromechanical model for the CFM layer. In this model, the 3D equivalent response of the CFM layer is generated from a weighted average of two alternating layers. The first is a matrix-mode layer, which is modeled using a unit-cell where the fibers are completely surrounded by a matrix phase. The second is a UC model for a fiber-mode layer, in which the

matrix medium does not completely shield the fibers, and both constituents have the same average strains.

The 3D stress-strain constitutive characterization for the fiber and matrix constituents is performed at the lowest level of the nested modeling framework. In the current study, the fiber can be modeled as a linear orthotropic material (isotropic for the case of E-glass). The J2 plasticity theory is used to model the nonlinear response for the matrix constituents. It should be noted that the material models for the subcells in the two main UCs are assumed to have the same basic fiber and matrix material behavior.

SUBLAMINATE MODEL: EQUIVALENT CONTINUUM FOR ROVING AND CFM LAYERS

The sublaminate model is derived from the application of an equivalent continuum concept. An equivalence between the actual sublaminate and an equivalent homogeneous continuum is defined using certain selected patterns of stress and strain. The 3D lamination theory in this derivation uses the same basic assumptions that are used by Pagano (1974) and Sun and Li (1988). A nonlinear model is derived by Haj-Ali and Pecknold (1996), with an efficient stress-update algorithm. This update algorithm is needed in the case where a nonlinear response is present at the matrix constituents of the different layers. The following derivation is for a sublaminate model with two layers, the roving and CFM.

The stress and strain vectors for each layer are transformed to material coordinates and are partitioned into in-plane and out-of-plane components

$$\bar{\sigma}_i = \{\sigma_{11} \ \sigma_{22} \ \tau_{12}\}, \quad \bar{\sigma}_o = \{\sigma_{33} \ \tau_{13} \ \tau_{23}\} \quad (1)$$

$$\bar{\epsilon}_i = \{\epsilon_{11} \ \epsilon_{22} \ \gamma_{12}\}, \quad \bar{\epsilon}_o = \{\bar{\epsilon}_{33} \ \gamma_{13} \ \gamma_{23}\} \quad (2)$$

where the overbars indicate homogenized sublaminate quantities.

Perfect bond is assumed between adjacent layers. Displacement continuity requires that the in-plane strains (ϵ_{11} , ϵ_{22} , γ_{12}) be continuous across the interface, and equilibrium of tractions across the interface requires that out-of-plane stresses (σ_{33} , τ_{13} , τ_{23}) be continuous across the interface. Unlike the 3D lamination theory, classical lamination theory for thin sections ignores the second interface condition and assumes that the out-of-plane stresses are negligible.

The in-plane strains and out-of-plane stresses are assumed to be the same throughout the sublaminate

$$\bar{\sigma}_o = \sigma_o^{(C)} = \sigma_o^{(R)} \quad (3)$$

$$\bar{\epsilon}_i = \epsilon_i^{(C)} = \epsilon_i^{(R)} \quad (4)$$

where (C) and (R) denote CFM and roving layers, respectively.

The complementary stresses and strains may differ in the roving and CFM layers. The homogenized in-plane stresses and out-of-plane strains are taken as weighted averages using the relative CFM and roving thickness t_C and t_R , respectively, as

$$\bar{\sigma}_i = \frac{1}{(t_C + t_R)} (t_C \sigma_i^{(C)} + t_R \sigma_i^{(R)}) \quad (5)$$

$$\bar{\epsilon}_o = \frac{1}{(t_C + t_R)} (t_C \epsilon_o^{(C)} + t_R \epsilon_o^{(R)}) \quad (6)$$

Eqs. (3)–(6) completely characterize the sublaminate model. It should be noted that there are no explicit material constitutive relations to satisfy at the sublaminate level. These calculations are done for the individual subcells within the UC models of the roving and the CFM. The roving and CFM sequence information is not preserved in this procedure. How-

ever, these effects are not expected to dramatically alter the structural response, especially if more elements are used through the thickness. In the case where this sequence is important, the sublaminar model is not used and each layer through the cross section is sampled to form the equivalent response by numerical integration in a ply-by-ply approach.

MICROMECHANICAL MODEL FOR ROVING LAYER

The roving layer is idealized as a doubly periodic array of rectangular cross-section fibers embedded in the matrix. The long fibers are aligned in the x_1 -direction. The other cross-section directions are referred to as the transverse directions. The rectangular unit cell geometry is shown in Fig. 2. The UC is divided into four subcells with constant deformation cells. Therefore, the traction and displacement continuity between the subcells, homogenization stress, and strain paths are not satisfied spatially; instead, the relevant average stress and strain components are used to satisfy these continuity constraints in an average sense.

The notation for the stress and strain vectors, defined in this section, are

$$\sigma_i^{(\alpha)} = [\sigma_{11}, \sigma_{22}, \sigma_{33}, \tau_{12}, \tau_{13}, \tau_{23}]^T \quad i = 1, \dots, 6 \quad (7a)$$

$$\varepsilon_i^{(\alpha)} = [\varepsilon_{11}, \varepsilon_{22}, \varepsilon_{33}, \gamma_{12}, \gamma_{13}, \gamma_{23}]^T \quad \alpha = 1, \dots, 4 \quad (7b)$$

where (α) denotes the subcell number in the UC; and i denotes the stress or strain component. These are also referred to herein as mode i .

The total volume of the unit cell is taken to be equal to one. The relative volumes of the four subcells are

$$v_1 = hb, v_2 = (1 - h)b, v_3 = h(1 - b), v_4 = (1 - h)(1 - b) \quad (8)$$

The axial strains are the same in all the subcells. Therefore, the longitudinal relations (mode 1) are

$$\varepsilon_1^{(1)} = \varepsilon_1^{(2)} = \varepsilon_1^{(3)} = \varepsilon_1^{(4)} = \bar{\varepsilon}_1^{(R)} \quad (9a)$$

$$v_1 \sigma_1^{(1)} + v_2 \sigma_1^{(2)} + v_3 \sigma_1^{(3)} + v_4 \sigma_1^{(4)} = \bar{\sigma}_1^{(R)} \quad (9b)$$

Consideration of the interfaces with normals in the x_2 -direction yields the traction continuity conditions for in-plane stress components 22 and 12, respectively. The corresponding strain compatibility conditions for these modes follow from separately considering subcells (1) and (2), and subcells (3) and (4), respectively. These relations are expressed for the direct stress component 22 (mode 2), as

$$\sigma_2^{(1)} = \sigma_2^{(2)} \quad (10a)$$

$$\sigma_2^{(3)} = \sigma_2^{(4)} \quad (10b)$$

$$\frac{v_1}{v_1 + v_2} \varepsilon_2^{(1)} + \frac{v_2}{v_1 + v_2} \varepsilon_2^{(2)} = \bar{\varepsilon}_2^{(R)} \quad (10c)$$

$$\frac{v_3}{v_3 + v_4} \varepsilon_2^{(3)} + \frac{v_4}{v_3 + v_4} \varepsilon_2^{(4)} = \bar{\varepsilon}_2^{(R)} \quad (10d)$$

For in-plane shear (mode 4), the relations are

$$\sigma_4^{(1)} = \sigma_4^{(2)} \quad (11a)$$

$$\sigma_4^{(3)} = \sigma_4^{(4)} \quad (11b)$$

$$\frac{v_1}{v_1 + v_2} \varepsilon_4^{(1)} + \frac{v_2}{v_1 + v_2} \varepsilon_4^{(2)} = \bar{\varepsilon}_4^{(R)} \quad (11c)$$

$$\frac{v_3}{v_3 + v_4} \varepsilon_4^{(3)} + \frac{v_4}{v_3 + v_4} \varepsilon_4^{(4)} = \bar{\varepsilon}_4^{(R)} \quad (11d)$$

Consideration of the interfaces with normals in the x_3 -direction yields the traction continuity conditions for out-of-plane stress components 33 and 13, respectively. The corresponding

strain compatibility conditions for these modes follow from separately considering subcells (1) and (3), and subcells (2) and (4), respectively. These relations are expressed for the direct stress component 33 (mode 3), as

$$\sigma_3^{(1)} = \sigma_3^{(3)} \quad (12a)$$

$$\sigma_3^{(2)} = \sigma_3^{(4)} \quad (12b)$$

$$\frac{v_1}{v_1 + v_3} \varepsilon_3^{(1)} + \frac{v_3}{v_1 + v_3} \varepsilon_3^{(3)} = \bar{\varepsilon}_3^{(R)} \quad (12c)$$

$$\frac{v_2}{v_2 + v_4} \varepsilon_3^{(2)} + \frac{v_4}{v_2 + v_4} \varepsilon_3^{(4)} = \bar{\varepsilon}_3^{(R)} \quad (12d)$$

For the out-of-plane shear component 13 (mode 5), the relations are

$$\sigma_5^{(1)} = \sigma_5^{(3)} \quad (13a)$$

$$\sigma_5^{(2)} = \sigma_5^{(4)} \quad (13b)$$

$$\frac{v_1}{v_1 + v_3} \varepsilon_5^{(1)} + \frac{v_3}{v_1 + v_3} \varepsilon_5^{(3)} = \bar{\varepsilon}_5^{(R)} \quad (13c)$$

$$\frac{v_2}{v_2 + v_4} \varepsilon_5^{(2)} + \frac{v_4}{v_2 + v_4} \varepsilon_5^{(4)} = \bar{\varepsilon}_5^{(R)} \quad (13d)$$

Finally, in the transverse shear mode, the traction continuity at all the interfaces between the subcells must be satisfied. Since the subcells have a constant stress, the relations for the transverse shear 23 (mode 6), are expressed as

$$\sigma_6^{(1)} = \sigma_6^{(2)} = \sigma_6^{(3)} = \sigma_6^{(4)} \quad (14a)$$

$$v_1 \varepsilon_6^{(1)} + v_2 \varepsilon_6^{(2)} + v_3 \varepsilon_6^{(3)} + v_4 \varepsilon_6^{(4)} = \bar{\varepsilon}_6^{(R)} \quad (14b)$$

Eqs. (8)–(14) completely define the relations of the stresses in the subcells of the roving layers. These relations are used in incremental (rate) form when the constitutive relations in the four subcells are nonlinear. Detailed algebraic derivations for different stiffness and compliance integration algorithms can be found in Haj-Ali and Pecknold (1996).

MICROMECHANICAL MODEL FOR CFM LAYER

The CFM layer is considered as a medium where resin is reinforced with mats of long swirly filaments randomly distributed in the plane of the layer. Therefore, the CFM effective medium can be represented with an in-plane isotropic model. A 3D-type UC is not possible due to the random distribution of the fibers. An in-plane stiffness equation for such a medium was derived by Tsai and Pagano (1968), by integrating over all possible in-plane orientations of the stiffness of a unidirectional lamina. Christensen and Waals (1972) derived the effective stiffness of a medium with complete 3D random orientation of fibers dispersed in the matrix. Their derived formulas reduce to those of Tsai and Pagano for the case of a medium with in-plane random reinforcement.

The goal of the present work is to derive a model that is able to predict the effective mechanical properties and the nonlinear stress-strain response due to matrix softening. This requires the knowledge of the average stress and strain in the constituents. The effective properties of the CFM model (Haj-Ali et al. 1998) compares well with those generated from the equations of Tsai and Pagano (1968). The CFM model generates 3D equivalent response for the CFM layer by a weighted average of two UC models for idealized alternating layers. The first is a matrix-mode layer (transverse), which is modeled using a unit-cell where the fibers are completely surrounded by a matrix phase. The second is a model for a fiber-mode layer (unidirectional layer), in which the fibers are not

shielded by the matrix, and both constituents have the same average strains.

The CFM unit-cell model is shown in Fig. 2 as a collection of four subcells. It is also constructive to note that the matrix-mode layer (part A) is composed of subcells (1) and (2), while the fiber-mode layer (part B) is composed of subcells (3) and (4). The out-of-plane direction is represented by the x_3 -axis. Through the CFM unit cells, the formulation is presented in terms of average stress and strains of subcells A and B. The fiber volume fractions within these parts should satisfy

$$\frac{V_1}{V_1 + V_2} = h = v_{fc}, \quad \frac{V_4}{V_3 + V_4} = \xi = v_{fc} \quad (15)$$

Considering parts A and B as layers, similar to the above sublaminar model, similar equations for the out-of-plane traction continuity and interface displacement continuity [(3) and (4)] are expressed

$$\bar{\sigma}_0^{(C)} = \sigma_0^{(A)} = \sigma_0^{(B)} \quad (16a)$$

$$\bar{\epsilon}_i^{(C)} = \epsilon_i^{(A)} = \epsilon_i^{(B)} \quad (16b)$$

The homogenized in-plane stresses and out-of-plane strains are taken as weighted averages using the fiber volume fraction in the CFM as

TABLE 1. Elastic Properties and Matrix Nonlinear Ramberg-Osgood Parameters

Mechanical property	Effective Modulus (msi)			Poisson's Ratio		Nonlinear Parameter (ksi)		
	E_1	E_2	G_{12}	ν_{12}	ν_{23}	β	n	τ_0
E-glass fiber	10.5	10.5	4.2	0.25	0.25	—	—	—
Vinylester resin	0.730	—	—	0.25	—	1.0	4.0	7.0

Note: Fiber volume fraction: roving layers = 0.407; CFM layers = 0.305.

TABLE 2. Predicted and Experimental Cross-Section Elastic Properties

Value	Effective Modulus (msi)						Poisson's Ratio		
	E_1	E_2	E_3	G_{12}	G_{13}	G_{23}	ν_{12}	ν_{13}	ν_{23}
Experimental Camp.	2.800	1.838	—	0.645	—	—	0.260	—	—
Experimental Tens.	2.633	1.486	—	0.645	—	—	0.300	—	—
Micromodel	2.825	1.783	1.287	0.662	0.434	0.411	0.275	0.295	0.316

$$\bar{\sigma}_i^{(C)} = \frac{1}{V} (V_A \sigma_i^{(A)} + V_B \sigma_i^{(B)}) \quad (17a)$$

$$\bar{\epsilon}_0^{(C)} = \frac{1}{V} (V_A \epsilon_0^{(A)} + V_B \epsilon_0^{(B)}) \quad (17b)$$

Within part A (subcell A), the following relations should be satisfied:

$$\bar{\sigma}^{(A)} = \sigma^{(1)} = \sigma^{(2)} \quad (18a)$$

$$\bar{\epsilon}^{(A)} = \frac{1}{V_A} (V_1 \epsilon^{(1)} + V_2 \epsilon^{(2)}) \quad (18b)$$

The analogous equations for part B are

$$\bar{\sigma}_0^{(B)} = \sigma_0^{(3)} = \sigma_0^{(4)} \quad (19a)$$

$$\bar{\epsilon}_i^{(B)} = \epsilon_i^{(3)} = \epsilon_i^{(4)} \quad (19b)$$

$$\bar{\sigma}_i^{(B)} = \frac{1}{V_B} (V_3 \sigma_i^{(3)} + V_4 \sigma_i^{(4)}) \quad (19c)$$

$$\bar{\epsilon}_0^{(B)} = \frac{1}{V_B} (V_3 \epsilon_0^{(3)} + V_4 \epsilon_0^{(4)}) \quad (19d)$$

Eqs. (15)–(19) define the relations of the average stresses and strains in the subcells of the CFM layer. These relations are used in an incremental (rate) form when the constitutive relations in the four subcells are nonlinear.

NUMERICAL IMPLEMENTATION OF MODEL

For finite strain increments and a nonlinear material response, the tangential stresses and strains typically violate the nonlinear constitutive relations of the subcell materials. In order to satisfy the actual stress-strain relationships as well as the traction and compatibility constraints, a stress update algorithm is needed. Both stiffness-based and compliance-based correction schemes have been developed. The stress update algorithm consists of two steps: (1) a predictor step, which may be a tangential or a trial elastic predictor; (2) followed by a correction step, in which the trial elastic state is adjusted in order to arrive at accurate stress values. Using a predictor step alone, without subsequent correction, may lead to unacceptable accumulation of error. The numerical implementation of the nonlinear equation for different micromodels is presented in Haj-Ali and Pecknold (1996).

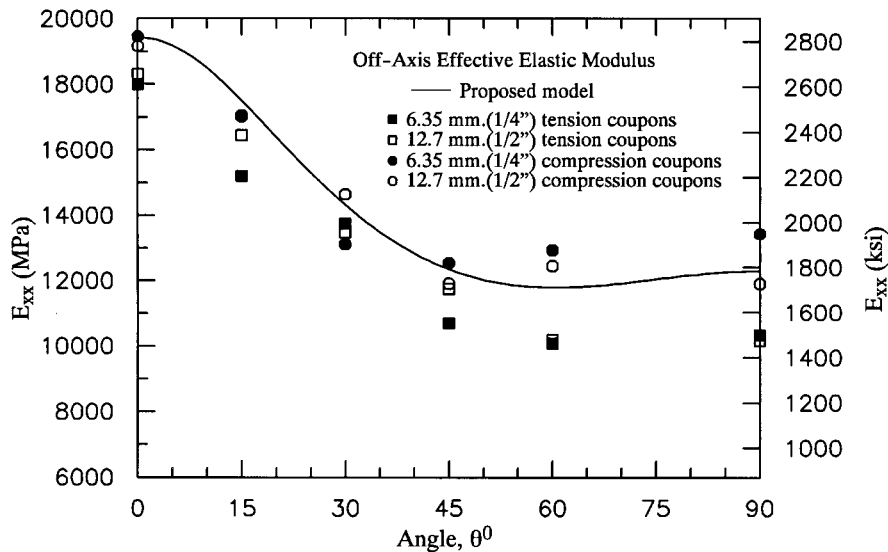


FIG. 3. Prediction of Off-Axis Elastic Stiffness of Coupons in Tension and Compression

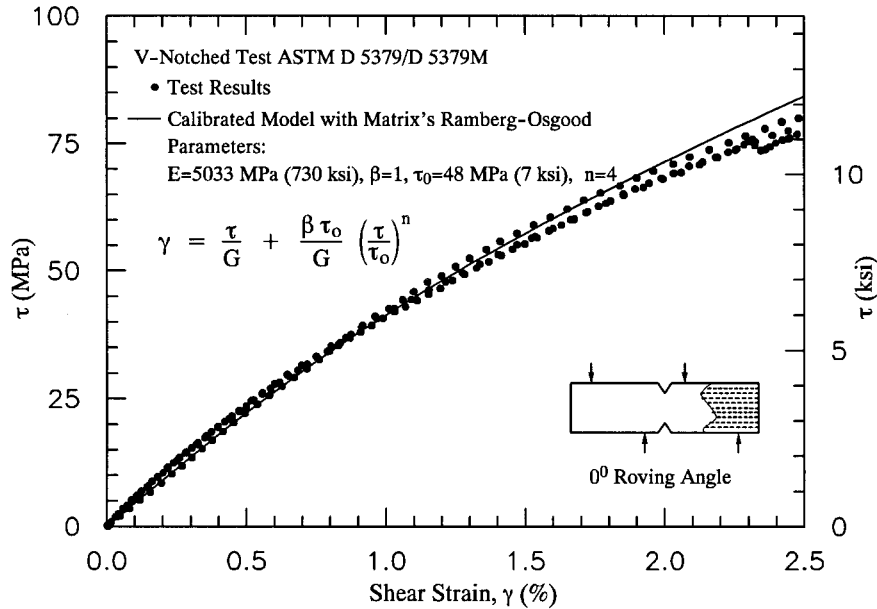


FIG. 4. Nonlinear Axial Shear Response of Pultruded Coupon Used for Calibrating Nonlinear Response of Matrix

EFFECTIVE MECHANICAL PROPERTIES: CALIBRATION AND PREDICTION

The micromodels are calibrated in the elastic range from known or assumed elastic properties of the matrix, the fiber, their fiber volume fractions, and the relative thickness of the roving and CFM layers. Table 1 shows typical mechanical properties of the E-glass fiber and the vinyl ester resin. The computed effective moduli and Poisson's ratios of the pultruded material, from the rovings/CFM sublaminate model, are reported in Table 2. The predicted values from the present analytical model compare favorably with those obtained experimentally. The lower experimental values of stiffness are due to opening of existing voids and microcracks under tensile load.

Ninety-six coupon tests are carried out to characterize the off-axis stiffness and the nonlinear stress-strain behavior of pultruded composites. These coupons are cut from 6.35 mm (1/4-in.) and 12.7 mm (1/2-in.) thick plates with different off-axis angles for the roving (0° , 15° , 30° , 45° , 60° , and 90°). These are subject to both tension and compression loading. The experimental results, in the form of elastic modulus for the off-axis coupons, are presented in Fig. 3. The prediction of the model is plotted by solid lines. The model provides a good prediction of the stiffness in compression when compared with stiffness from off-axis tests. The stiffness from off-axis tension tests is lower than those obtained from compressive tests. This decrease is more pronounced as the off-axis angle increases. The difference in stiffness can be attributed to material imperfections such as existing voids and microcracks and the presence of fillers in the resin matrix. These imperfect effects are not considered in the current formulation and add to the reliability of the proposed model.

NONLINEAR STRESS-STRAIN RESPONSE: CALIBRATION AND PREDICTION

V-notch shear test results are used to calibrate the nonlinear matrix behavior. The J2 deformation theory is used along with the Ramberg-Osgood uniaxial representation for the nonlinear behavior. It should be mentioned that both matrix constituents, in the roving and CFM micromodels, are assumed to have the same elastic and nonlinear parameters. Fig. 4 illustrates the pronounced nonlinear axial-shear stress-strain response of this material. The matrix Ramberg-Osgood stress-strain is cali-

brated by varying its parameters until the overall response is matched with the V-notch test results. Once the nonlinear response is calibrated, as shown in Table 2, the calibration of the proposed model is complete.

Next, the prediction capability of the proposed model for pultruded composites is examined for off-axis coupons that are

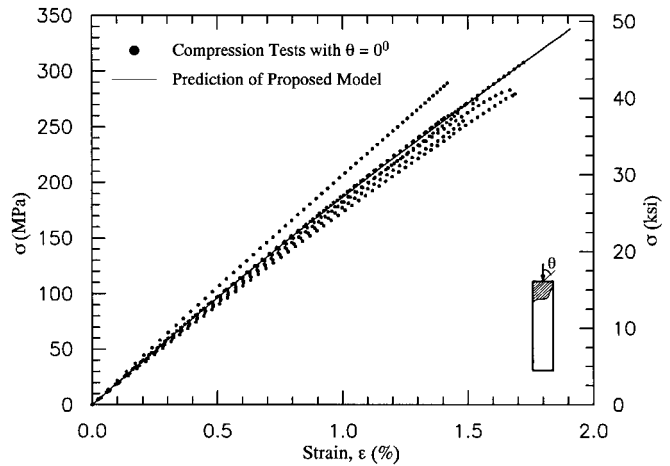


FIG. 5. Prediction of Off-Axis Compressive Response for 0°

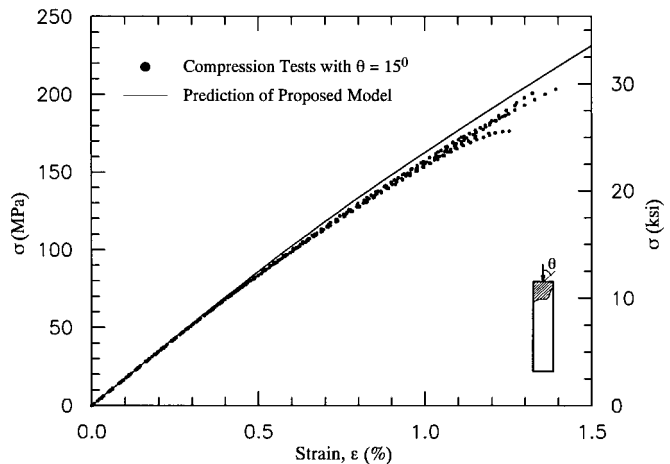


FIG. 6. Prediction of Off-Axis Compressive Response for 15°

subject to compressive loading. Figs. 5–10 show the experimental results (with repeated tests) and the prediction of the model (solid line). Different observations can be made. The nonlinear prediction capability of the model compares very well with the test results. The last point in the plotted results is the ultimate failure point. Nonlinear response is evident even in the case of unidirectional roving reinforcement, as shown in Fig. 5. This may be explained by the relatively low overall FVF (0.34). These results reinforce the validity of the proposed nonlinear modeling formulation for these pultruded materials.

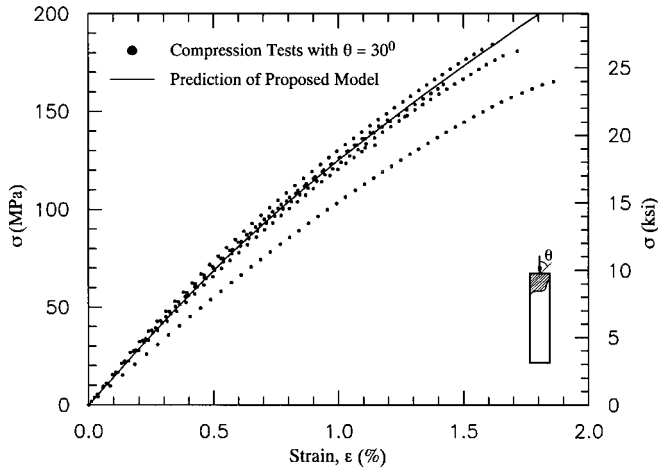


FIG. 7. Prediction of Off-Axis Compressive Response for 30°

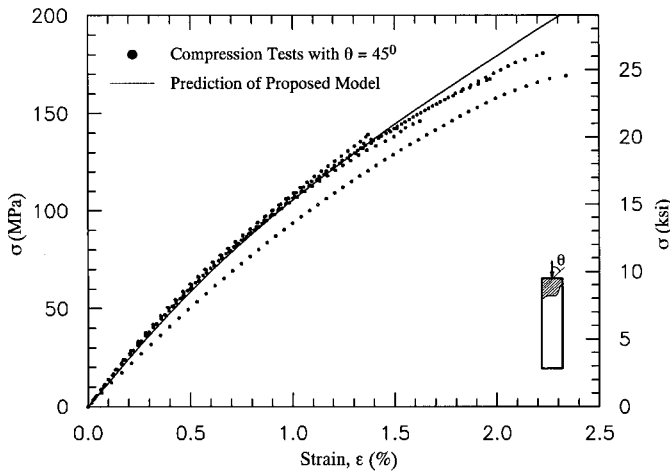


FIG. 8. Prediction of Off-Axis Compressive Response for 45°

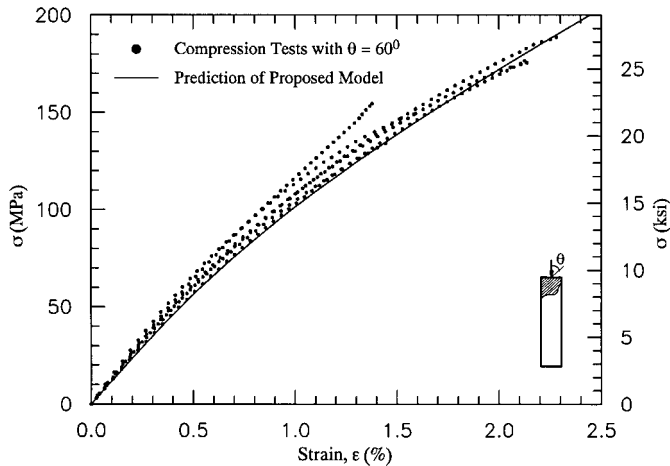


FIG. 9. Prediction of Off-Axis Compressive Response for 60°

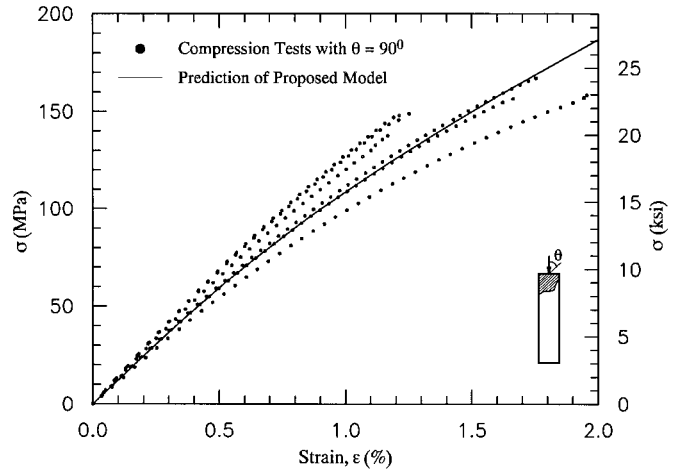


FIG. 10. Prediction of Off-Axis Compressive Response for 90°

CONCLUSIONS

A new 3D micromechanical framework for pultruded composite materials is derived. The proposed modeling framework employs a nested multiscale approach that can include different micromodels for the layers within the cross section of the composite. The CFM and roving micromodels can explicitly recognize the response of the fiber and matrix at their lower level of hierarchy. The proposed model can predict the overall nonlinear behavior of pultruded composite materials under a general multiaxial state of loading. Coupon tests are used to experimentally verify the analytical results. The model demonstrates accurate predictions for the effective elastic properties, as well as for the off-axis nonlinear compressive response up to ultimate failure. The framework can be easily incorporated within a classical displacement-based FE structural modeling, using 3D continuum or shell-type elements.

ACKNOWLEDGMENT

This work was supported by the National Science Foundation through the Civil and Mechanical Systems Division under Grant No. 9876080.

REFERENCES

- Aboudi, J. (1991). *Mechanics of composite materials—A unified micromechanical approach*, Elsevier Science, New York.
- Bank, L., and Yin, J. (1999). "Failure of web-flanged junction in post-buckled pultruded I-beams." *J. Compos. for Constr.*, ASCE, 3(4), 177–184.
- Barbero, E. J. (1991). "Pultruded structural shapes—From the constituents to the structural behavior." *SAMPE J.*, 27, 25–30.
- Binshan, S. Y., Svenson, A. L., and Bank, L. C. (1995). "Mass and volume fraction properties of pultruded glass fibre composites." *Comp.*, 26, 725–731.
- Christensen, R. M., and Waals, F. M. (1972). "Effective stiffness of randomly oriented fibre composites." *J. Comp. Mat.*, 6, 518–532.
- Haj-Ali, R. M., and Pecknold, D. A. (1996). "Hierarchical material models with microstructure for nonlinear analysis of progressive damage in laminated composite structures." *Struct. Res. Ser. No. 611, UILU-ENG-96-2007*, Department of Civil Engineering, University of Illinois at Urbana-Champaign, Urbana, Ill.
- Haj-Ali, R. M., Zureick, A. H., Kilic, M. H., and Steffen, R. (1998). "Micromechanics-based 3-D nonlinear analysis of pultruded composite structures." *Proc., Int. Conf. on Computational Engrg. Sci., ICES'98*, Atluri, S. N. ed., 1526–1533.
- Herakovitch, C. T., and Mirzadeh, F. (1991). "Properties of pultruded graphite/epoxy." *J. Reinforced Plastics and Compos.*, 10, 2–28.
- Luciano, R., and Barbero, E. J. (1994). "Formulate for the stiffness of composites with periodic microstructure." *Int. J. Solids and Struct.*, 31(21), 2933–2944.
- Mottram, J. T. (1992). "Lateral-torsional buckling of a pultruded I-beam." *Compos.*, 23(2), 81–92.
- Mottram, J. T. (1993). "Short and long term structural properties of pul-

- truded beam assemblies fabricated using adhesive bonding." *Comp. and Struct.*, 25, 387–395.
- Pagano, N. J. (1974). "Exact moduli of anisotropic laminates." *Mechanics of composite materials*, G. P. Sendeckyj, ed., Academic, San Diego, 23–44.
- Smith, S. J., Parsons, I. D., and Hjelmstad, K. D. (1998). "An experimental study of the behavior of connections for pultruded GFRPI-beams and rectangular tubes." *Comp. and Struct.*, 42, 281–290.
- Smith, S. J., Parsons, I. D., and Hjelmstad, K. D. (1999). "Finite element and simplified models of GFRP connections." *J. Struct. Engrg.*, ASCE, 125(7), 749–756.
- Sonti, S. S., and Barbero, E. (1996). "Material characterization of pultruded laminates and shapes." *J. Reinforced Plastics and Compos.*, 15, 701–717.
- Sun, C. T., and Li, S. (1988). "Three-dimensional effective elastic constants for thick laminates." *J. Comp. Mat.*, 22, 629–639.
- Tsai, S. W., and Pagano, N. J. (1968). "Invariant properties of composite materials." *Composite Materials Workshop*, S. W. Tsai, J. C. Halpin, and N. J. Pagano, eds., Technomic Publishing Co., Lancaster, Pa., 233–253.
- Turvey, G. J. (1998). "Torsion tests on pultruded GRP sheet." *Comp. Sci. and Technol.*, 58, 1343–1351.
- Vakanier, A. R., Zureick, A., and Will, K. M. (1991). "Prediction of local flange buckling in pultruded shapes by finite element analysis." *Proc., Spec. Conf. Advanced Compos. Mat. in Civ. Engrg. Struct.*, ASCE, Material Engrg. Division, S. L. Iyer and R. Sen, eds., N.Y., 302–312.
- Wang, Y., and Zureick, A. (1994). "Characterization of the longitudinal tensile behavior of pultruded I-shape structural members using coupon specimens." *Comp. and Struct.*, 29, 463–472.
- Zureick, A., Kahn, L. F., and Bandy B. J. (1995). "Tests on deep I-shape pultruded beams." *J. Reinforced Plastics and Compos.*, 14, 378–389.